ELECTROSTATIC FORCES IN MUSCLE AND CYLINDRICAL GEL SYSTEMS

B. M. Millman and B. G. Nickel, *Biophysics Interdepartmental Group, Department of Physics, University of Guelph, Guelph, Ontario, N1G 2W1, Canada*

ABSTRACT   Repulsive pressure has been measured as a function of lattice spacing in gels of tobacco mosaic virus (TMV) and in the filament lattice of vertebrate striated muscle. External pressures up to ten atm have been applied to these lattices by an osmotic stress method. Numerical solutions to the Poisson-Boltzmann equation in hexagonal lattices have been obtained and compared to the TMV and muscle data. The theoretical curves using values for κ calculated from the ionic strength give a good fit to experimental data from TMV gels, and an approximate fit to that from the muscle lattice, provided that a charge radius for the muscle thick filaments of ~ 16 nm is assumed. Variations in ionic strength, sarcomere length and state of the muscle give results which agree qualitatively with the theory, though a good fit between experiment and theory in the muscle case will clearly require consideration of other types of forces. We conclude that Poisson-Boltzmann theory can provide a good first approximation to the long-range electrostatic forces operating in such biological gel systems.

INTRODUCTION

In 1961, Bernal and Fankuchen published their classic study of hexagonally-packed gels of rod-shaped viruses and suggested that the stability of such gels resulted from a balance between electrostatic repulsive and van der Waals attractive forces, even over distances of several hundred ångstroms. Elliott (1968) attempted an approximate numerical calculation of these forces for the muscle filament lattice, based on theory developed by Derjaguin and Landau (1941) and Verwey and Overbeek (1948), and concluded (partly as a result of using too large a value for the Hamaker constant) that an electrostatic-van der Waals force balance could account for the observed lattice spacings. These calculations have since been improved (Brenner and McQuarrie, 1973; Brenner and Parsegian, 1974), and in their recent work, Parsegian and Brenner (1976) found that one could not reconcile the predictions of an improved theory with the Bernal and Fankuchen (1941) data on equilibrium spacings in TMV gels. They called for further experimentation under conditions where theory and measurement could be expected to agree.

In an attempt to gain insight into the nature of the forces in these systems, we began a systematic experimental study of lattice spacing as a function of pressure in both TMV gels and muscle. We used the experimental method recently developed by LeNeveu et al. (1976) whereby an external osmotic pressure is generated by solutions of large, inert, uncharged polymeric molecules. We have correlated our data with calculations of the purely electrostatic pressure in these systems on the assumption that the measurements correspond to an intermediate pressure regime where the weak van der Waals forces are negligible and the strong "hard core" overlap repulsive forces are still absent. Initial results from the muscle

system have been reported briefly (Millman and Racey, 1977; Millman and Wakabayashi, 1979) and detailed accounts of experimental results on muscle in rigor,[1] on resting muscle,[2] and on TMV gels,[3] are in preparation.

METHODS

Osmotic Pressure Determination

Samples of vertebrate striated muscle and of TMV gels were subjected to a net external pressure by means of the osmotic pressure exerted by solutions of large polymeric molecules (LeNeveu et al., 1976). The polymeric molecules used (Dextran from BDH or Pharmacia Chemical Co., Pistcataway, N. J.; polyvinylpyrrolidone [PVP] from Sigma Chemical Co., St. Louis, MO.) are uncharged, chemically-inert molecules. Because of their large size, they are unable to penetrate the hexagonal lattices of either the virus gels or the muscle filaments.

The osmotic pressure generated by the polymer solutions was measured directly by the method of LeNeveu et al. (1976), using the membrane osmometer designed by R. P. Rand (Brock University) and used for the osmotic pressure determinations in that paper. Osmotic pressure was determined as a function of polymer concentration across a dialysis membrane (Spectrapor 2: Spectrum Medical Industries Inc., Los Angeles, Calif.). Polymer concentration was monitored by its refractive index using a sugar refractometer. In any particular experiment, the refractive index of the polymer solution was measured after equilibration of the system to enable a direct conversion into osmotic pressure.

In most of our experiments, we used dextran with a molecular weight range from 200,000 to 270,000. In experiments with both muscle and TMV gels, some results were obtained with a dialysis membrane (similar to that used to calibrate osmotic pressure) separating the dextran solution from the sample. These results were indistinguishable from those obtained without the membrane, showing that the polymer molecules do not enter the hexagonal lattices. Essentially identical results were also obtained in the muscle system with solutions made with PVP (average molecular weight = 40,000).

Lattice Spacing

Lattice spacings were measured by low-angle x-ray diffraction using mirror-monochromator cameras similar to those used by Huxley and Brown (1967), with specimen-to-film distances between 20 and 40 cm. The cameras were mounted either on an Elliott GX6 rotating anode (Elliott Automation, Boehrum Wood, England) or on a Jarrell-Ash microfocus x-ray generator (Spectro Equipment, Royalton, Ohio). Exposures of a few hours were usually required for the TMV gels; of less than one hour for the muscle except for very high polymer concentrations, where exposures of a few hours were sometimes necessary. The x-ray beam ($CuK_{\alpha 1}$) passed through a 1–2 mm thick sample bounded by thin mica (TMV) or Mylar (muscle) windows. TMV patterns were obtained at room temperature; muscle patterns at room temperature for most rigor muscles, or at 8°C in the case of relaxed muscles.

Equatorial x-ray reflections from the hexagonal lattices were obtained. Normally, the 10, 11, and 20 reflections were seen from the TMV gels and the 10, and 11 reflections from the muscle filament lattice, though other orders were seen occasionally in both types of sample after long x-ray exposures. In both cases, changes produced in the lattice spacing were reversible.

TMV Gels

TMV was grown on young tomato plants, harvested, and purified by the method of Gregory and Holmes (1965). The final purification was done in sodium phosphate buffer of ionic strength 0.1 M and pH of either 6 or 7.2. After final centrifugation, a small part of the pellet was placed, along with a small amount of buffer, in a circular chamber (volume ~$5\mu l$). A thin sheet of mica covered one side of the sample, and a single sheet of dialysis membrane covered the other side. About 2 ml of test solution (dextran dissolved in buffer) was placed over the dialysis membrane and the sample was allowed to equilibrate for a few hours to several days. Before examination on the x-ray camera, most of the dextran

---

[1]Millman, B. M., K. Wakabayashi, and T. J. Racey. Manuscript in preparation.

[2]Millman, B. M., and T. Irving. Manuscript in preparation.

[3]Millman, B. M., T. Irving, B. G. Nickel, and M. Loosley-Millman. Manuscript in preparation.

solution was removed, leaving a small volume above the dialysis membrane, which was then covered with a second thin mica sheet and sealed. The final polymer concentration was determined by measuring the refractive index of the solution just before sealing the sample chamber.

In some samples, the dialysis membrane was omitted, allowing direct contact between the polymer solution and the TMV sample. No difference was detected between results from these preparations and those where dialysis membrane was used.

Muscle Preparation

Glycerol-extracted rabbit psoas muscle was prepared by the method of Rome (1967). For experimental use, small strips ($\sim 1 \times 2$ mm in cross section and 1–2 cm long) were removed, tied to small plastic frames, and equilibrated in standard salt solution (100 mM KCl, 1mM $MgCl_2$, 6.7 mM KPO_4 buffer:pH 7.0). After equilibration for periods from one to several hours, the standard salt solution was replaced by a polymer solution (dextran dissolved in standard salt solution) of volume several times the volume of the muscle sample. The muscle was then left to equilibrate for several hours. Muscles prepared in this manner were in rigor.

Fresh frog sartorius or semitendinosus muscles were mounted in a chamber of capacity of ~ 25 ml and adjusted to the desired sarcomere length as determined by light diffraction. Muscle preparations in rigor could be obtained consistently by exposing the fresh muscle to 4 mM idoacetate in Ringer's solution for 48 h at 4°C before skinning. The muscle was then chemically skinned with detergent (Triton X1000) using a technique described by Racey (1976). The muscle was placed in a "skinning" solution (0.1–0.5% Triton dissolved in a "rigor" solution: 100 mM KCl, 4 mM $MgCl_2$, 10 mM histidine buffer:pH 7.0) for 1–8 h, and then rinsed in the rigor solution for ~ 1 h. This solution was then exchanged for solution containing a specific concentration of polymer, and the preparation was allowed to equilibrate for 2–24 h. Relaxed muscles were skinned by a similar method, except that the "relaxing" solution also contained 5 mM $MgCl_2$, 5 mM ATP, and 5 mM EGTA. In this case 0.5% Triton was used at pH 6.5 for 3–8 h. During treatment with skinning, relaxing and polymer solutions, the relaxed preparation was constantly agitated with a magnetic stirrer. This technique, similar to that used by Magid and Reedy (1980), usually gave relaxed muscle preparations, though on occasion the muscle had moved into rigor as judged by the relative intensity of the 10 and 11 equatorial x-ray reflections. (In the relaxed muscle $I_{10} > I_{11}$; in muscle in rigor $I_{10} < I_{11}$.)

Rabbit psoas muscle in rigor was also obtained by skinning intact muscle strips in the manner described for frog muscle after the muscle had passed into rigor by leaving it at room temperature for a few hours. No iodoacetate of glycerol extraction was needed in this case.

CALCULATION OF ELECTROSTATIC PRESSURE

Our theoretical calculations of the electrostatic pressure are based on solutions of the Poisson-Boltzmann equation:

$$\nabla^2 \psi = -(4\pi e/\epsilon) \Sigma Z_i n_i^0 e^{-Z_i e\psi/kT} \tag{1}$$

in a region of dielectric constant ϵ between periodic arrays of cylinders of dielectric constant $\hat{\epsilon}$ and a fixed surface charge density. The ions are specified by a charge $Z_i e$ and a number density n_i^0 in the reservoir region. Elsewhere the ions move in an average electrostatic potential ψ but are otherwise noninteracting. Although this approximation is known to be quantitatively inaccurate when applied to the calculation of the thermodynamic properties of ionic solutions with ionic strengths > 0.01 M, it is believed to be rather accurate for the long-range correlation functions. This evidence is based both on Monte Carlo studies (Torrie and Valleau, 1979), and on approximate integral equation solutions of model systems. For example, the solution for the mean spherical approximation (MSA) to a model 1–1 ionic solution of ions with hard core repulsive diameters, d, predicts an inverse screening length $\kappa(1 + 1/4 \ \kappa^2 d^2 - 1/6 \ \kappa^3 d^3 + ...)$ where κ is the Debye-Hückel parameter (cf. Eq. 4a below) (Waisman and Lebowitz, 1972). For typical ionic diameter $d \sim 0.4$ nm and $\kappa \sim 1.0$ nm^{-1}

appropriate to a 0.1 M solution, the MSA yields only a 4% correction to the simple Poisson-Boltzmann result. Since at higher ionic concentrations the MSA is in reasonable agreement with Monte Carlo results (Rasaiah et al., 1972), we believe a figure of $< 5\%$ as a reasonable estimate of the accuracy of the Poisson-Boltzmann equation for the range of parameters of experimental interest here. The experimental data we present cannot distinguish such small corrections to the screening length.

Once the electrostatic potential in Eq. 1 has been calculated, the local ionic number density and pressure are determined by:

$$n_l = \Sigma \, n_i^0 e^{-Z_i e\psi/kT}, \qquad P_l = n_l kT. \qquad (2)$$

However, the total force perpendicular to any plane surface in the medium includes extra terms arising from the local electric fields. These Maxwell stress tensor terms are given by $\epsilon(E_\parallel^2 - E_\perp^2)/8\pi$, where $E_\parallel$ and $E_\perp$ are the components of $-\nabla\psi$ parallel and perpendicular to the surface. The bulk or macroscopic pressure P above ambient for the periodic arrays considered here is then just the local force per unit area averaged over the surface of a unit cell in the sample. That is,:

$$P = (\langle n_l \rangle - \Sigma \, n_i^0)kT + (\epsilon/8\pi) \, \langle E_\parallel^2 - E_\perp^2 \rangle. \qquad (3)$$

We have considered in detail the two systems shown in Fig. 1. For the simple hexagonal (TMV) system we write $\psi = \Sigma_n \, \alpha_n \, r^{6n} \cos 6n\theta$ inside each cylinder and $\psi = \Sigma_n \, F_n(x) \cos 6n\theta$ in the interstitial region within each unit cell. We have defined a "radial" coordinate $x = \ln r \cdot (3 + \beta \cos 6\theta)/(1 - \beta \cos 6\theta)$ with β a numerical constant chosen to fix the points A and B in Fig. 1 at the same maximum x value. The Poisson-Boltzmann equation then becomes a set of coupled, nonlinear, ordinary differential equations for $F_n(x)$ which we have solved numerically subject to the boundary conditions that the discontinuity in the perpendicular component of $D/4\pi = \epsilon E/4\pi$ on the cylinder surface gives the fixed surface charge density σ and that the perpendicular component of E vanishes on the surface segment A–B in Fig. 1. We have typically achieved better than 4–figure accuracy with a truncated set of from 5 to 10 coupled equations. The change of variable from r to x indicated above was crucial in enabling us to obtain such convergence even at close packing, i.e., nearest neighbor cylinder spacing $C = 2a$, where a is the cylinder radius.
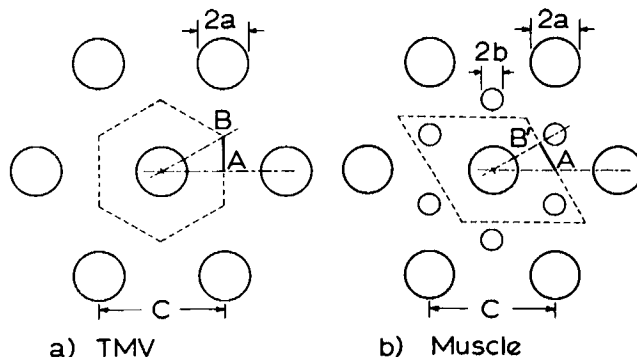

a) TMV   b) Muscle

Figure 1   Geometric details of the model systems considered in this paper. Regions enclosed by dashed lines are the unit cells. Because of symmetry the solid segments A–B and A–B' are the only portions of these boundaries that need be considered when calculating the macroscopic pressure via the average given in Eq. 3 or 7.

The solutions to the Poisson-Boltzmann equation for the TMV system are conveniently characterized by two dimensionless products. One, $a\kappa$, involves the Debye-Hückel parameter κ:

$$a\kappa = a \cdot \left(\frac{4\pi e^2}{\epsilon kT} \sum Z_i^2 n_i^0\right)^{1/2}, \tag{4a}$$

and the other, λ, involves the cylinder surface charge density σ, or number of electronic charges per unit length ν:

$$\lambda = a \cdot \frac{4\pi e |\sigma|}{\epsilon kT} = \frac{2e^2 |\nu|}{\epsilon kT} \tag{4b}$$

We must also specify the ratios of the reservoir ionic densities n_i^0 and the ratio of the inside to screening medium dielectric constants $\hat{\epsilon}/\epsilon$. The results are quite insensitive to this latter ratio, and we have simply used the value $\hat{\epsilon}/\epsilon = 0.2$ for all calculations. Our results are displayed in plots of the dimensionless pressure $a^2 P/f_0$ vs. cylinder separation $C/2a$, where the constant f_0 is given by:

$$f_0 = \epsilon(kT)^2/8\pi e^2 \approx 2.26 \times 10^{-8} \text{ dynes} \tag{5}$$

for $\epsilon = 80$ and $T = 293°K$. We find the pressure as shown in Fig. 2 falls off approximately as
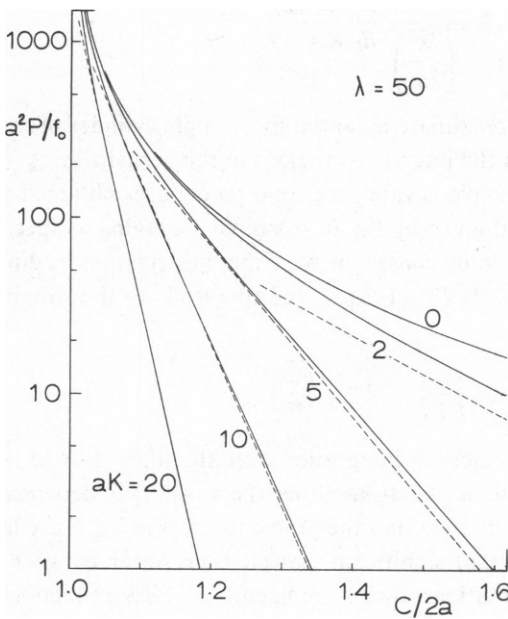

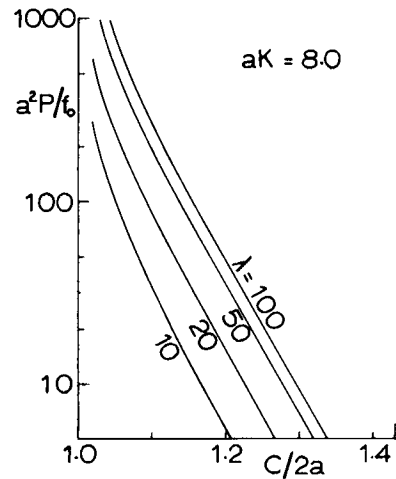Figure 2   Figure 3

Figure 2   Pressure as a function of cylinder separation for the simple hexagonal (TMV) system. Curves are distinguished by different $a\kappa$ for a monovalent ionic solution. The surface charge parameter is $\lambda = 50$ corresponding to a cylinder charge of ~ 35 e/nm. Solid curves are the exact solutions to the Poisson-Boltzmann Eq. 1; dashed curves are the approximate solutions determined from Eqs. 6 and 7.

Figure 3   Pressure as a function of cylinder separation determined from the exact solution of Eq. 1 for the TMV system screened by a monovalent ionic solution with $a\kappa = 8.0$. Curves are labeled by different cylinder surface charge λ defined by Eq. 4b. The upper curve corresponds to 70 e/nm, and the lower curve to 7 e/nm. The saturation of the pressure for large λ closely follows Eq. 8a.

exp$[-\kappa(C - 2a)]$ as expected on the basis of simple Debye-Hückel screening theory. Furthermore, the behavior of the pressure with surface charge density as shown in Fig. 3 can readily be understood in terms of the one-dimensional solutions to the Poisson-Boltzmann equation as discussed below.

It is possible to simplify these pressure calculations considerably and to extend them to the idealized muscle system if both the cylinder radii and the separation between all cylinder surfaces is greater than the Debye-Hückel screening length κ^{-1}. These criteria are definitely satisfied for the parameters of experimental interest here; quantitative comparisons of the simplified solutions described below with the exact calculation on the TMV system for some typical conditions are shown in Fig. 2. Our approximation is based on the observation that even in the presence of extremely large surface charge densities, the potential ψ around any one cylinder becomes small enough beyond a distance κ^{-1} of the surface that the linearized Poisson-Boltzmann, i.e., Debye-Hückel, equation is valid. Then the only difference between the exact and linearized solutions in this small ψ region is a scale factor. Furthermore, if $a\kappa >$ 1, the region where ψ is large is effectively planar and we can use the Poisson-Boltzmann equation in one dimension to estimate this scale factor.

Finally, our experimental conditions are such that the analytical formula for monovalent solutions is reasonable; that is, ψ(Poisson-Boltzmann)$/\psi$(Debye-Hückel) $=$ $2/[1 + \sqrt{1 + (\lambda/2a\kappa)^2}]$ far from the planar surface. We take κ from Eq. 4a, multiply the Debye-Hückel solution in two dimensions by this scale factor, and thus write:

$$\frac{e\psi_a}{kT} = - \frac{2}{1 + \sqrt{1 + \left(\frac{\lambda}{2a\kappa}\right)^2}} \frac{\lambda_a}{a\kappa} \frac{K_0(r\kappa)}{K_1(a\kappa)}, \tag{6}$$

where the K_i are Bessel functions, as our approximate potential for a single cylinder of radius a and surface charge parameter λ_a. Since in the interstitial regions in the periodic system the potential is small and the superposition principle is valid, the total potential is obtained by a summation over all cylinders of the potential given by Eq. 6. A simple averaging as specified by Eq. 3 then gives the pressure. However, to be consistent with the linearization leading to Eq. 6, we must keep only terms to order $(e\psi/kT)^2$ in Eq. 3 and this leads to the simplified expression:

$$\frac{P}{f_0} = \left\langle \kappa^2 \left(\frac{e\psi}{kT}\right)^2 + \left(\nabla_\parallel \frac{e\psi}{kT}\right)^2 - \left(\nabla_\perp \frac{e\psi}{kT}\right)^2 \right\rangle. \tag{7}$$

The averaging in Eq. 7 was obtained by numerical integration over the lines A–B or A–B' shown in Fig. 1, and we kept contributions to $e\psi/kT$ from either the 4 or 6 cylinders nearest these line segments. The reader should be cautioned that the gradient terms in Eq. 7 are large along A-B'; for the muscle calculation and that significant cancellations occur between the various terms. Therefore no further approximations, such as replacing the Bessel functions by their asymptotic formulae, can be tolerated in this case.

On the other hand, reasonable simplifications of Eqs. 6 and 7 can be made in the TMV case which, except for the scale factor, will lead to the formulae in the literature. In particular, if we include contributions to $e\psi/kT$ from the two cylinders nearest A–B only, drop the gradient terms in Eq. 7, and replace $K_0(r\kappa)$ by its asymptotic value $\sqrt{\pi/2r\kappa}\exp{(-r\kappa)}$, then we obtain:

$$\frac{a^2 P}{f_0} \approx \left(\frac{2}{1 + \sqrt{1 + \left(\frac{\lambda}{2a\kappa}\right)^2}}\right)^2 \left(\frac{\lambda}{K_1(a\kappa)}\right)^2 \frac{2\sqrt{3}}{C} \int_0^{C/2\sqrt{3}} dx \frac{2\pi}{r\kappa} e^{-2r\kappa}, \tag{8a}$$

where $r = \sqrt{(C/2)^2 + x^2}$. The last factor in Eq. 8a is approximately:

$$\frac{2\sqrt{3}}{C} \int_0^\infty dx \frac{4\pi}{\kappa C} e^{-\kappa C - 2\kappa x^2/C} = \sqrt{3} \left(\frac{2\pi}{\kappa C}\right)^{3/2} e^{-\kappa C}, \tag{8b}$$

in agreement with the asymptotic result given by Brenner and Parsegian (1974). For the range of parameters shown in Fig. 2, the pressure determined from Eq. 8a,b is indistinguishable from that given by Eqs. 6 and 7.

Two points related to the scale factor are worth noting. First, for our experimental conditions, the use of the full nonlinear Poisson-Boltzmann equation leads to pressure estimates anywhere from a factor of 4 to 50 lower than those given by the linear Debye-Hückel theory. Second, the nonlinear Poisson-Boltzmann equation predicts that the pressure will saturate as $\lambda \rightarrow \infty$ (see Eq. 8a) and be relatively insensitive to surface charge density whenever $\lambda/(2a\kappa) > 1$.

Since this is precisely our experimental regime we conclude that our largest uncertainties in the experimental fits are the cylinder radii rather than the very poorly known surface changes. By reversing the argument we note the experimental pressure measurements cannot be used to determine the surface charge density but can be used to estimate the radii.

RESULTS

TMV Gels

About one-half of the TMV gels made as described above and allowed to equilibrate for one to several days gave clear low-angle x-ray diffraction patterns. The better patterns showed sharp rings corresponding to the 10, 11, and 20 reflections from a hexagonal lattice of size ~26 nm. Thus, as found by Bernal and Fankuchen (1941), the TMV particles form sizable microcrystals, with the rod shaped virus particles oriented parallel to each other in the hexagonal lattice. There is, however, no overall orientation to the microcrystals and they thus give powder x-ray diffraction patterns.

On exposure to dextran solutions, the TMV lattice was maintained, but the interparticle spacing was reduced depending on the net osmotic pressure of the solution (Fig. 4). The relation between lattice shrinking and osmotic pressure was nonlinear, decreasing towards a limiting inter rod spacing of ~17 nm. Taking $a = 8.5$ nm as the charge radius of the virus rods, we have plotted the data for pH $= 7.2$, $I = 0.10$ M in Fig. 5 in the dimensionless parameters described earlier. The solid curve is the theoretical calculation with the appropriate $\kappa = 1.04$ nm^{-1} and $\lambda = 50$, corresponding to an assumed charge density of ~ 35 e/nm. The curve is in apparent agremeent with the data points over a pressure range of more than two orders of magnitude. The values for a and λ are reasonably close to those expected for TMV at this pH. Note particularly that this curve contains no adjustable parameters other than a and λ, and that, for a given λ, the data determines a to better than 5%.

As noted above, changes in the charge density λ produce little shift in the theoretical curves. A series of measurements at pH 6.0, which gave a curve indistinguishable from the curve at pH 7.2, is consistent with the expected insensitivity to λ. However, scatter of the data points probably masked any small change caused by the resulting surface charge differences. Current experiments are underway using larger pH differences and differences in ionic strength; we hope that these new measurements will show clearly different force vs. distance behavior.
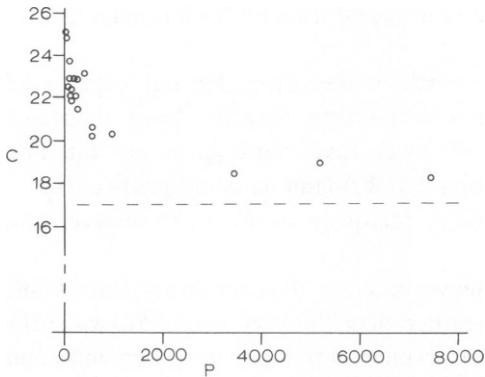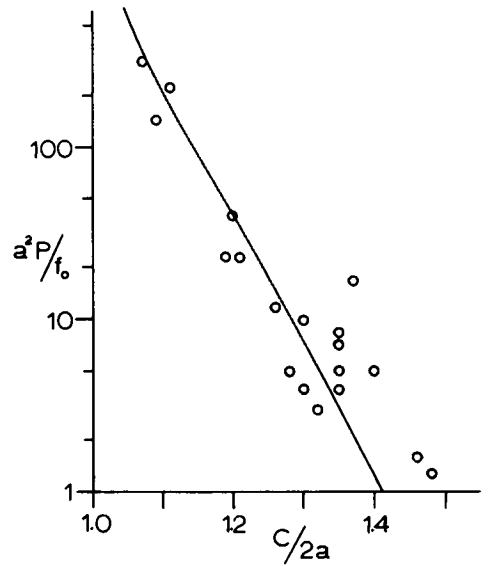
Figure 4

Figure 5

Figure 4   The decrease of interrod spacing, C(nanometers) with increased osmotic pressure, P(torr) in TMV gels. Each point represents a single measurement. The dashed line represents the minimum interrod spacing for large pressure.

Figure 5   The relationship between pressure and interrod spacing in dimensionless parameters (a^2P/f_o and $C/2a$, respectively) for the TMV data in Fig. 4, with $a = 8.5$ nm. The solid line is the exact solution of Eq. 1 for $a\kappa = 8.8$ and $\lambda = 50$. The reservoir ionic concentrations are in the ratio $[+e] : [-e] : [-2e] = 3:1:1$, appropriate to sodium phosphate buffer.

Muscle Filament Lattice

In the skinned muscle preparations, whether the membranes were removed by glycerol extraction or by chemical skinning, the filament lattice shrank when exposed to polymer solutions. As in the case of the TMV gels, the amount of lattice shrinking was related in a nonlinear fashion to the net osmotic pressure of the polymer solution. In the muscle case, shrinking below an interfilament spacing between the thick filaments of ~32 nm was not observed, even with osmotic pressures as high as 10 atm. A similar limit of osmotic shrinking has been observed in intact muscle using glucose, sucrose or small ions as osmotic agents.[4]

The muscle filament lattice is considerably more complex than the lattice of TMV gels. In intact muscle, thick (myosin) filaments form an hexagonal array with an interfilament spacing which decreases in frog muscle from ~450 to 350 nm as the sarcomere length increases from 2.0 to 3.6 μm (Elliott et al., 1963). Thin (actin) filaments sit at the trigonal points of the lattice in an overlap region which varies linearly from 1.6μm at a sarcomere length of 2.0 μm to zero at a sarcomere length of 3.6 μm. For purposes of comparison with theory, we have calculated the pressure for both structures shown in Fig. 1 and then summed the results with a weighting that varies linearly with the fractional overlap of actin and myosin. Our procedure suggests that at all but the very longest sarcomere lengths, the elctrostatic forces are dominated by repulsion between the thick and thin filaments.

Electron microscope photographs suggest a backbone radius for the thick filaments of 6 to 7.5 nm with projections (cross-bridges) sticking out a further 10 nm or so (Huxley, 1972). The
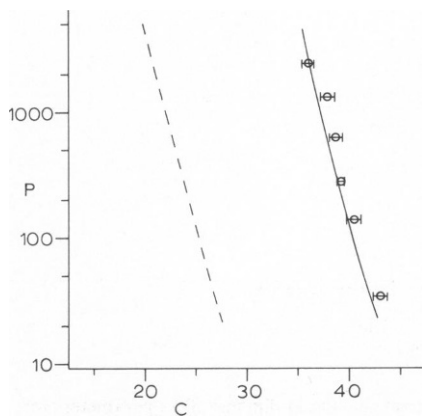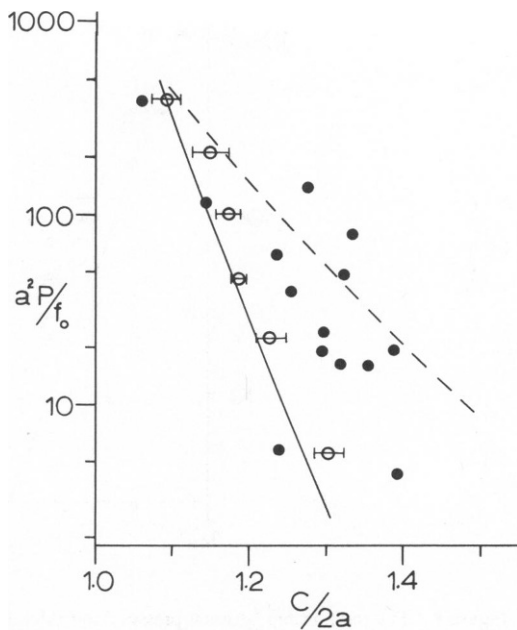

Figure 6

Figure 7

Figure 6   The relationship between pressure P(torr) and thick filament spacing C(nanometers) for rabbit psoas muscle in rigor solution at sarcomere lengths from 2.5 to 3.1 μm. Each point represents the average from 3–13 measurements together with its standard error. The lines are theoretical curves calculated from Eq. 6 and 7 for $\kappa = 1.09$ nm^{-1}, $\lambda_a = 150$, $\lambda_b = 27$, $b = 3.0$ nm, and a sarcomere length of 2.8 μm; the dashed line is for $a = 7.5$ nm, the solid line for $a = 16.5$ nm.

Figure 7   The relationship between pressure and thick filament spacing in dimensionless parameters for rabbit psoas muscle at sarcomere lengths from 2.5 to 3.1 μm. The open circles show the same data as Fig. 6. Solid circles represent individual measurements obtained in rigor solution diluted tenfold. The lines are theoretical curves; the solid line is as in Fig. 6, and the dashed line for $\kappa = 0.35$ nm^{-1}, appropriate to the diluted solution.

thin filament is smoother with a radius between 2.5 and 4 nm. It is likely, based on known amino acid compositions of the various parts of the myosin molecule, that most of the charge on the thick filament lies on the backbone.[5] Measurements of filament charge per unit length of the filament have been made by Naylor and Elliott;[6] we have used figures of ~100 and 20 e/nm for the thick and thin filaments, respectively, appropriate to our experimental conditions.

Using the above values for filament charge and radii ($a = 7.5$ nm, $b = 3.0$ nm), the calculated curve for electrostatic pressure as a function of filament separation (dashed line) and a typical set of experimental measurements (rabbit psoas muscle in rigor at moderately long sarcomere lengths) are shown in Fig. 6. The experimental points lie nowhere near the calculated curve; in fact, they lie in a "forbidden" region of the plane corresponding to forces which no amount of charge could produce. The only way to reconcile the data to the calculations, if indeed the forces involved are electrostatic, is to assume that the charge must be at a much larger radius than previously thought. Thus, for example, if the charges on the thick filaments are at a radius of 16.5 nm, ~double that previously assumed, then the

---

[5]Elliott, G. F. Personal communication.
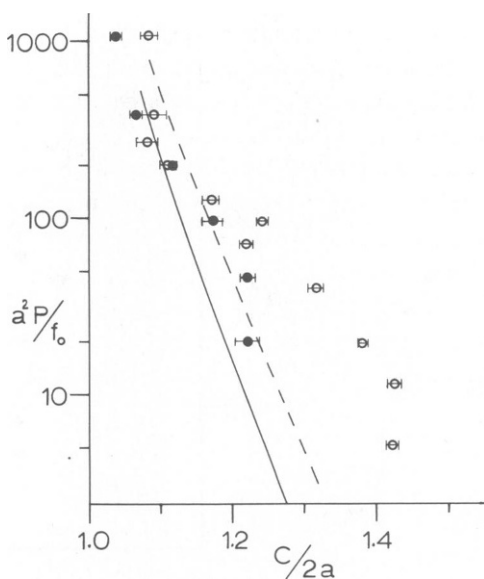[6]Naylor, G. R. S., and G. F. Elliott. Manuscript submitted for publication.

Figure 8   The relationship between pressure and thick filament spacing in dimensionless parameters for frog muscle in rigor. The circles show averaged results with standard errors at two different sarcomere lengths assuming $a = 15.5$ nm. Open circles: 2.1–2.5 μm; solid circles: 3.1–3.4 μm. The lines are theoretical curves for $a = 15.5$ nm, $b = 2.8$ nm, $\kappa = 1.16$ nm^{-1}, $\lambda_a = 150$, $\lambda_b = 27$; at sarcomere lengths of 2.3 μm (dashed line) and 3.2 μm (solid line).

experimental points are in reasonable agreement with the calculated curve (solid line, Fig. 6). The data for frog muscle are similar and indicate an $a = 15.5$ nm. Such large radii are surprising, but in the remainder of this paper we have used these values for a, and have attempted to check this model for consistency by varying the experimental conditions of pH, ionic strength, and filament overlap. Note that in both cases any agreement between the experimental and theoretical electrostatic pressure is lost if the above values for the charge radii are changed by more than ~1 nm. The implications of this finding for the structure of the thick filament will be discussed in Millman and Elliott.[7]

As our first check, we have done experiments using solutions of different pH and ionic strength. Shifting the pH to 8.0 produced data which did not differ significantly from that at pH 7.0. As in the case of the TMV gels we find this hardly surprising, given the large experimental scatter and the small shift of the theoretical curves which occurs with changes in filament charge. Decreasing the ionic strength by a factor of 10 gave an increased pressure for a given interfilament separation, shifting the curve to the right, much as predicted by the theory (Fig. 7). In this case, however, agreement between the experimental points and the theoretical curve is not so good.

Because of the change in overlap pattern with sarcomere length, one would expect the electrostatic pressure to decrease as the sarcomere length increased at a particular interfilament spacing. Fig. 8 shows data from frog muscle in rigor at short and moderately long sarcomere lengths together with the theoretical curves for these two conditions. While neither set of data fits the theoretical curve very well, the data from the short muscles depart significantly from the theoretical predictions, particularly at low osmotic pressures. This may

---

[7]Millman, B. M., and G. F. Elliott. Manuscript in preparation.

indicate, in part, that other force systems are coming into play. In particular, there may be considerable resistance to shrinking provided by the cross-bridges which are known to link thick and thin filaments during rigor. This effect wll be greatest at short sarcomere lengths where filament overlap is greatest, and will decrease as the sarcomere length increases. This appears to be so at moderate and high pressures as demonstrated by data, taken in collaboration with T. Irving, on relaxed frog muscle at short sarcomere lengths which show a smaller interfilament spacing in relaxed muscle than was found in muscle in rigor at the same net osmotic pressure. Alternatively, the large charge radius we have found for the thick filaments could indicate a less rigid structure for these filaments. A decrease of ~10% in charge radius with increasing pressure would bring our data into line with the theoretical curves. Thus electrostatic forces may still be the dominant force system, coupled with a variable charge radius.

DISCUSSION

The results from TMV gels indicate that the Poisson-Boltzmann equation (Elliott, 1968; Brenner and Parsegian, 1974) can provide a good first approximation to the electrostatic forces acting in hexagonally-packed cylindrical systems where the particle dimensions and separations may be 10 nm or more. Application to the muscle filament lattice shows general agreement, though in this complex system there are clearly more factors which have to be taken into account

Under our experimental conditions, particularly in the case of muscle, other nonelectrostatic forces may be involved, especially at very high and very low pressures. At high pressures, the rods may come into direct contact with each other or with tightly bound water layers, giving rise to additional stereochemical or hydration pressures. At low pressures, resistance to indefinite swelling does occur, as shown by the fact that both TMV gels and muscle filament lattices reach equilibrium spacings when there is no external pressure, i.e., no polymer in the external solution (Bernal and Fankuchen, 1941; Matsubara and Elliott, 1971). These other forces could include physical attachments (e.g., Z line and M line in muscle), cross-linking attachments (especially in rigor muscle), volume constraints from the experimental chamber, and van der Waals attractive forces. If, as we believe, we can now measure repulsive forces and accurately calculate the electrostatic forces, it should be possible to identify some of these other stabilizing forces.

In the case of the TMV gels we have obtainted reasonable quantitative agreement between our experimental data and the theoretical curves. We are extending and refining our experiments on both TMV and muscle; in particular, we are studying the effect of varying the pH and ionic strength. Results from these experiments should enable us to test the Poisson-Boltzmann theory over a broader range of conditions.

Of particular interest in the muscle case are the changes that occur on contraction. We already have indications of differences between relaxed and rigor muscle, and similar changes may occur between relaxed and contracting muscle. We intend to compare relaxed and contracting muscle for information about the lateral forces in the living muscle filament lattice (e.g., Schoenberg, 1980). It is quite conceivable that clues to the mechanism of muscular contraction will emerge from these studies.

REFERENCES

Bernal, J. D., and I. Fankuchen. 1941. X-ray and crystallographic studies of plant virus preparations. *J. Gen. Physiol.* **25:**111–146.

Brenner, S. L., and D. A. McQuarrie. 1973. Force balances in systems of cylindrical polyelectrolytes. *Biophys. J.* **13:**301–331.

Brenner, S. L., and V. A. Parsegian. 1974. A physical method for deriving the electrostatic interaction between rod-like polyions at all mutual angles. *Biophys. J.* **14:**327–334.

Derjaguin, B., and L. Landau. 1941. Theory of the stability of strongly charged lyophobic sols and of the adhesion of strongly charged particles in solutions of electrolytes. *Acta Physiochim. USSR.* **14:**633–692.

Elliott, G. F. 1968. Force-balance and stability in hexagonally-packed polyelectrolyte systems. *J. Theor. Biol.* **21:**71–87.

Elliott, G. F., J. Lowy, and C. R. Worthington. 1963. An x-ray and light diffraction study of the filament lattice of striated muscle in the living state and in rigor. *J. Mol. Biol.* **6:**295–305.

Gregory, J., and K. C. Holmes. 1965. Methods of preparing orientated tobacco mosaic virus sols for x-ray diffraction. *J. Mol. Biol.* **13:**796–801.

Huxley, H. E. 1972. Molecular basis of contraction in cross-striated muscles. *In* The Structure and Function of Muscle, Vol. 1. G. H. Bourne, editor. Academic Press, Inc., London. 301–387.

Huxley, H. E., and W. Brown. 1967. The low-angle x-ray diagram of vertebrate striated muscle and its behavior during contraction and rigor. *J. Mol. Biol.* **30:**383–434.

LeNeveu, D. M., R. P. Rand, and V. A. Parsegian. 1976. Measurement of forces between lecithin bilayers. *Nature (Lond.).* **259:**601–603.

Magid, A., and M. K. Reedy. 1980. X-ray diffraction observations of chemically skinned frog skeletal muscle processes by an improved method. *Biophys. J.* **30:**27–40.

Matsubara, I., and G. F. Elliott. 1972. X-ray diffraction studies on skinned single fibres of frog skeletal muscle. *J. Mol. Biol.* **72:**657–669.

Millman, B. M., and T. J. Racey. 1977. Osmotic shrinkage of the filament lattice in frog semitendinosus muscle. *Biophys. J.* **17:**175a. (Abstr.)

Millman, B. M., and K. Wakabayashi. 1979. Shrinking of the muscle filament lattice in polymeric solutions. *Biophys. J.* **25:**111a. (Abstr.)

Parsegian, V. A., and S. L. Brenner. 1976. The role of long range forces in ordered arrays of tobacco mosaic virus. *Nature (Lond.).* **259:**632–635.

Racey, T. J. 1976. The myofilament lattice: osmotic and ionic effects in the relaxed state and in rigor. M.Sc. Thesis, University of Guelph.

Rasaiah, J. C., D. N. Card, and J. P. Valleau. 1972. Calculation of the "restricted primitive model" for 1–1 electrolyte solutions. *J. Chem. Phys.* **56:**248–255.

Rome, E. 1967. Light and x-ray diffraction studies of the filament lattice of glycerol-extracted rabbit psoas muscle. *J. Mol. Biol.* **27:**591–602.

Schoenberg, M. 1980. Geometrical factors influencing muscle force development. II. Radial forces. *Biophys. J.* **30:**69–78.

Torrie, G. M., and J. P. Valleau. 1979. A Monte Carlo study of an electric double layer. *Chem. Phys. Lett.* **65:**343–346.

Verwey, E. J. W., and J. T. G. Overbeek. 1948. Theory of the stability of lyophobic colloids. Elsevier/North Holland, Amsterdam. 205.

Waisman, E., and J. L. Lebowitz. 1972. Mean spherical model integral equations for charged hard spheres. II. Results. *J. Chem. Phys.* **56:**3093–3099.

DISCUSSION

Session Chairman: V. Adrian Parsegian; *Scribe:* Kathy Jennison

SCHOENBERG: Would you amplify upon what you think some of the problems might be with the "worst fit" in the rabbit muscle? I believe it was the overlap experiments which led you to believe that perhaps the cross-bridges are not important; however, particularly in the case of the muscle in rigor, the projections from the thick filaments are bound rather strongly to the thin filaments. Would you comment on what effect that might have?

MILLMAN: I think you are referring to the experiments on frog muscle in rigor.

SCHOENBERG: Those seem to show the larger deviation from the theory than the rabbit does, for some reason.

MILLMAN: My feeling that the cross-bridges have a relatively small effect comes largely from recent data we have on relaxed muscle, and data shown in Fig. 9, which compares the relaxed and the rigor cases. The central part of the curves are the most significant from the standpoint of electrostatic theory. The lower points are close to equilibrium where van der Waals or other attractive forces are balancing the electrostatic repulsion; the upper points are where there may be steric contact between the filaments. Thus there are other force systems coming in at the extremes. Unlike the rabbit data (Fig. 6), neither set of points agrees well with the theoretical curves, perhaps because the thick filament radius is decreasing as the external pressure is increased. But the fact that the rigor and relaxed muscle curves are parallel over the whole pressure range is quite consistent with a simple change in charge radius. A similar conclusion comes from muscle stretched beyond filament overlap: a plot of a^2P/f_0 vs. $c/2a$ for such points would lie almost exactly over the relaxed points.

SCHOENBERG: Do you think van der Waals forces might be important under any conditions in either TMV or muscle, or do you think we can safely ignore these? What is the range of filament separations over which the electrostatic interaction energy is greater than KT, the thermal energy, in TMV and muscle?

MILLMAN: In both TMV and muscle over most of the range we are concerned with here ($c/2a$ between 1.1 and 1./4 nm), the calculated van der Waals pressure is one or two orders of magnitude smaller than the electrostatic pressure, and the thermal pressure one or two orders of magnitude smaller still (Fig. 10). Preliminary calculations from equilibrium spacings with no external pressure indicate that even at these positions the electrostatic repulsion is about five times the van der Waals attraction in both TMV and muscle. This implies that either van der Waals forces are not a major factor determining equilibrium, or the Hamaker constant we have used (7×10^{-14} ergs) is too small. This value for the Hamaker constant was actually derived for lipids, not for protein systems, and it may be that in proteins the Hamaker constant should be higher. I'm not an expert on Hamaker constants, and maybe somebody here can comment on this.

PARSEGIAN: A comment on van der Waals forces: there is no reason to expect a qualitative difference between protein systems and lipid systems for the magnitudes of these forces across water. There is great reason to worry
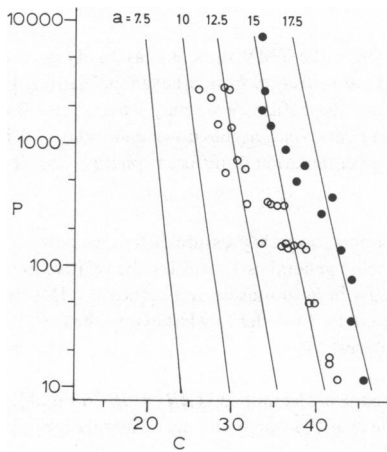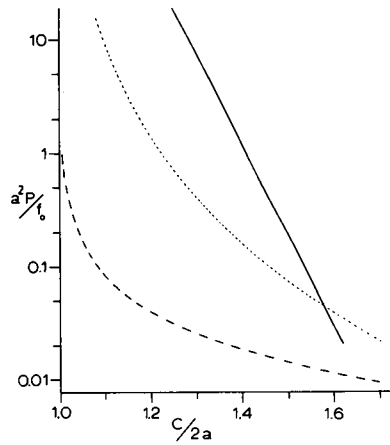

Figure 9

Figure 10

Figure 9   The relationship between pressure P (torr) and thick filament spacing C (nanometers) for frog sartorius muscle at sarcomere lengths between 2.0 and 2.5 μm. Solid circles: muscles in rigor, the same points as the open circles in Fig. 8. Open circles: relaxed muscles, each point representing an individual measurement. The lines are theoretical curves calculated as in Fig. 8 but for different values of a (in nanometers).

Figure 10   Electrostatic, van der Waals, and thermal pressure as a function of cylinder separation for the TMV system. Solid line: electrostatic pressure as calculated in Fig. 4. Dotted line: van der Waals pressure calculated for a = 8.5 nm and a Hamaker constant of 7×10^{-14} erg. Dashed line: thermal pressure calculated for cylindrical rods with a = 8.5 nm and length = 300 nm at a temperature of 20°C.

about extracting Hamaker coefficients in the region where you are looking. We have not done this with the membrane systems in that regime because the errors are so high; you have to bring the bodies a good bit closer with lower repulsive forces to get more reliable estimates. So don't worry too much about this discrepancy of your Hamaker estimates.

KORETZ: I wonder if the stiffness of the cross-bridges, which mechanically would be seen as an electrostatic repulsive force, is contributing to the non-ideality of the curves that you are getting — because you are getting an S-shaped curve for the frog sartorius muscle. Also I wonder about the agreement with theory as a function of sarcomere length or degree of overlap.

MILLMAN: To answer the second question first, the agreement with sarcomere length is consistent over a fairly extensive range of sarcomere lengths, i.e. where the curves agree at one sarcomere length they agree at the others; where they don't agree well at one sarcomere length, they don't agree very well at the others.

The S-shaped curves Dr. Koretz is referring to are in Fig. 8. My feeling is that this represents a change in the charge radius, which probably is close to the filament backbone. Although most of the charge on the muscle proteins appears to be on the backbone, we cannot at this stage eliminate the possibility that some substantial charge is on the cross-bridges, and that what we may be seeing here is a shift in the position of the cross-bridges as we compress the lattice. It is only at very high pressures (the top point of the curve) that the possibility of substantial mechanical resistance for the cross-bridges appears likely. Such a contribution at lower pressures would tend to bend the curve in the opposite direction to what is seen, i.e. increase the repulsive pressure at lower values of C.

BLOOMFIELD: In your calculations on a hexagonal lattice, you are assuming that the rods in fact remain co-linear. I can imagine small thermal oscillations where the ends would bump into each other. Does that affect the force balance at all?

MILLMAN: Here we are really talking about the thermal pressure; in the regime we are studying, that force is very small compared to the other forces.

MAKOWSKI: You said that you were selecting out for hexagonal phases in comparing the theory to your experiment with TMV; but TMV gels tend to be rather disordered. It is not going to be a good hexagonal array. How much is this disorder going to affect the calculations? Since the disorder is going to be of a different order of magnitude in muscle, is that going to change the comparison of theory and experiment in muscle, compared to the TMV?

MILLMAN: Within one small micro-crystal or micro-gel region in the TMV there is reasonably good order. The x-ray reflections we get are quite sharp and we see 1,0, 1,1, and 2,0 reflection from a hexagonal lattice. Frequently, however, we obtain patterns with only a single reflection, which may be diffuse, or we may see a sharp 1,0 with other, more diffuse, reflections. If we drop these latter results the experimental scatter goes down enormously. While we are not sure of all the reasons for this, we believe that they involve a combination of different phases, disordered phases and nonequilibrium states.

ELLIOTT: In your Eq. 3, the first (kT) term is related to the Donnan osmotic pressure difference between the phase containing the rods and the surrounding phase. Could you give some general estimates for the relative importance of the remaining, stress tensor, terms? I ask because experimentally in both muscle and cornea the Donnan pressure term seems to me to describe many aspects of the behavior adequately. I wonder to what extent the further terms are of practical importance, though clearly they are of theoretical interest.

MILLMAN: Since Eq. 3 only refers to the pressure along the edge of the unit cell (AB or AB' in Fig. 1), it does not relate directly to the Donnan pressure, which must be an average over the whole unit cell. The relative importance of the electrostatic and osmotic terms depends on the specific location in the unit cell. For example, consider the Debye-Hückel limit (Eq. 7) for two parallel plates separated by a distance d. Then $e\psi/kT$ varies as $\cosh(x - d/2)$ and the nonvanishing contributions to the pressure are the first and third terms, which give $P \alpha \cosh^2 \kappa(x - d/2) - \sinh^2\kappa(x - d/2) - 1$ i.e. P is independent of x. Clearly, at the midpoint ($x = d/2$), only the first term contributes; but for x near 0 or d, dropping the third term would yield nonsense if $\kappa >> 1$.

PARSEGIAN: Let's not forget that the whole point of the Poisson-Boltzmann equation is to keep electrochemical potentials constant throughout the system. The physical force does not depend on the particular mathematical stress surface chosen for computation.

ELLIOTT: I have the impression that you regard the electrostatic repulsive force as charge-saturated, i.e., further increases in the rod charge would not increase the repulsive force. Yet all the experimental results —(Rome, 1967

and 1968; Naylor and Elliott [in preparation]; and Elliott, 1980 [this volume])— suggest that at long sarcomere lengths, where the myosin-myosin interaction is dominating, the 1,0 spacing closely follows the myosin rod charge as the pH and ionic strength are changed. A similar situation applies in cornea, where in general the swelling rate, and the x-ray spacing achieved in a given time, increase with pH (above the isoelectric point) at a given ionic strength (Goodfellow et al., 1978); Elliott et al., 1980). Could you comment, please?

MILLMAN: In our particular experimental situation, we believe we were very close to charge saturation. I think the results you refer to are cases where the charge was reduced, not increased. Now, if you look at Fig. 3, the pressure curve for infinite charge would be slightly above the line for $\lambda = 100$. Our experiments are in a region quite close to that. By increasing our charge we would not expect to shift the curve very much. If, however, you were to decrease the charge by, say, a factor of two, the curve would shift to a greater extent. Because of the rather large scatter of our data in dextran, we find that we can barely detect these effects. But most of the experimentation which you, Dr. Rome and others have done has used the equilibrium lattice with no external pressure. Where there is less experimental manipulation, there is less scatter in the data, and changes can be picked up more precisely. We are now doing a series of experiments on such an equilibrium lattice, to investigate whether or not van der Waals forces are significant in the system. Here, we are getting significant differences as the charge (or pH) is varied, so there is no disagreement on this point.

PARSEGIAN: I believe that the saturability that you describe is evidence against the pure proportionality between charge and potential that is characteristic of a Donnan system. Typically, the Donnan expression is limited to cases in which the Debye lengths are comparable to distances between bodies, wherein you can speak of an average potential throughout. The opposite limit is when you have very wide variations in the potential. You may still speak of averages, and they may be good for certain things, but when you have charge saturation of the type you describe, and the screening lengths you see, you have quite a big variation in the potential through the space between charged bodies. A Donnan potential is not a good average for this potential.